Mono-X Signatures of a Fermionic Dark Matter at the LHC

Kai Ma[c†]

Collaborator(s): Shao-Feng Ge[a, b, ∗], *Lin-Yun He*[c, ‡], *Ning Zhou*[d,§]

† makai@ucas.ac.cn, ∗ gesf@sjtu.edu.cn, ‡ a1164432527@gmail.com, § nzhou@sjtu.edu.cn

[a] *Tsung-Dao Lee Institute & School of Physics and Astronomy*
[b] *Shanghai Key Laboratory for Particle Physics and Cosmology, Shanghai Jiao Tong University*
[c] *School of Physics, Shaanxi University of Technology*
[d] *Shanghai Jiao Tong University, Key Laboratory for Particle Astrophysics and Cosmology (MOE), SKLPPC, Shanghai*

Roadmap for DM Models for Run 3

May/15, 2024

Effective Operators

We are interesting following four-fermion contact couplings,

$$
\begin{aligned}
\mathcal{O}_{\mathcal{S}} &\equiv (\bar{q}q)\,(\bar{\nu}_{\mathcal{L}}\chi_{\mathcal{R}}) \ , \\
\mathcal{O}_{\mathcal{P}} &\equiv (\bar{q}i\gamma_5 q)\,(\bar{\nu}_{\mathcal{L}}\chi_{\mathcal{R}}) \ , \\
\mathcal{O}_{\mathcal{V}} &\equiv (\bar{q}\gamma_\mu q)\,(\bar{\nu}_{\mathcal{L}}\gamma^\mu\chi_{\mathcal{L}}) \ , \\
\mathcal{O}_{\mathcal{A}} &\equiv (\bar{q}\gamma_\mu\gamma_5 q)\,(\bar{\nu}_{\mathcal{L}}\gamma^\mu\chi_{\mathcal{L}}) \ , \\
\mathcal{O}_{\mathcal{T}} &\equiv (\bar{q}\sigma_{\mu\nu} q)\,(\bar{\nu}_{\mathcal{L}}\sigma^{\mu\nu}\chi_{\mathcal{R}}) \ ,
\end{aligned}
\tag{1}
$$

where the dark fermion (χ) is always accompanied by a SM neutrino (ν).

Collider Search (CS): **mono-X production**.

Direct Detection (DD): **absorption of the DM at nuclear target**.

Mono-γ @Collider Search

Feynman diagrams of the mono-γ process: **(a)** is for the signal operators, **(b)** is for the irreducible background.

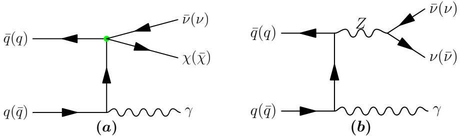

Normalized parton level distributions of θ_γ **(a)** and $p_{T,\gamma}$ **(b)** of the photons in the lab frame with center of mass energy $\sqrt{s} = 13\,\mathcal{TeV}$. **(c):** total cross sections as functions of $\sqrt{\hat{s}}$.

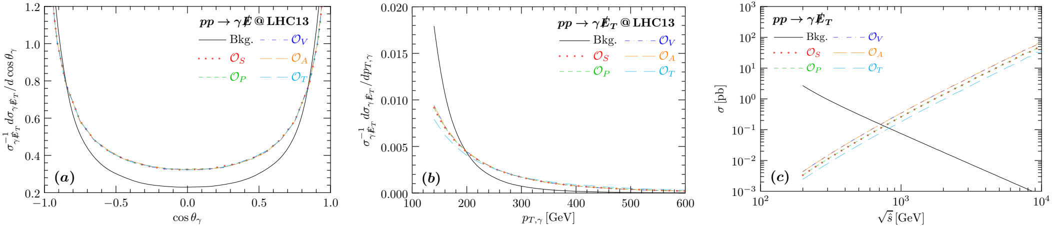

Mono-γ @Collider Search

Light panel: Validation of our simulation for the missing transverse momentum distribution. The experimental data are (black line) taken from the arXiv:2011.05259 [hep-ex], and our results (red triangle) have been renormalized by multiplying an overall constant. **Right panel**: Expected exclusion limits at 95% C.L. at the LHC with $\sqrt{s} = 13\,TeV$ and a total luminosity $\mathcal{L} = 139\ fb^{-1}$.

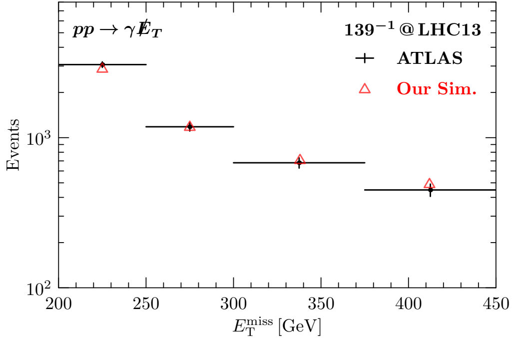

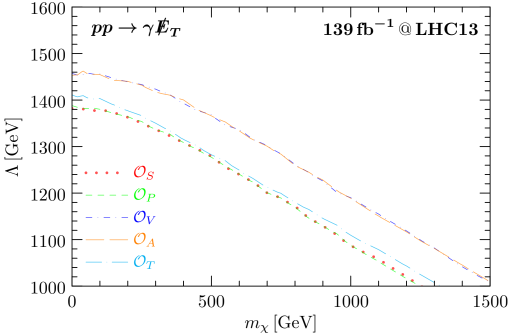

Mono-jet @Collider Search

Feynman diagrams contributing to the mono-jet events due to the signal operators. **(a)**, **(b)** and **(c)** for the signal operators, **(d)**, **(e)** and **(f)** for the irreducible background.

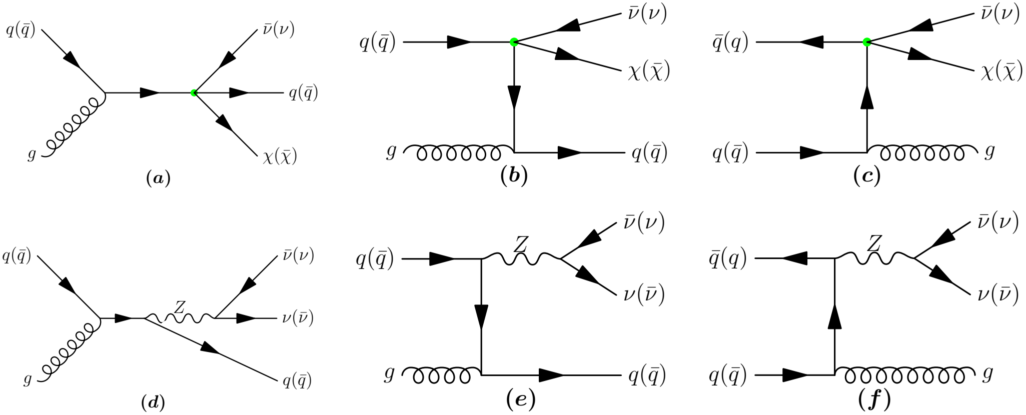

Mono-jet @Collider Search

Normalized parton level distributions of the polar angle (θ_j) **(a)** and transverse momentum ($p_{T,j}$) **(b)** of the jet in the lab frame with center of mass energy $\sqrt{s} = 13TeV$. **(c):** total cross sections of the background and signals as functions of the center-of-mass energy at parton level, $\sqrt{\hat{s}}$. In all the three panels, the signal (colorful non-solid curves) are shown for parameters $m_\chi = 0GeV$ and $\Lambda_i = 1TeV$, and the background (black-solid curve) stands for the irreducible contribution from the channel $q\bar{q}'/qg \to jZ(\nu\nu)$.

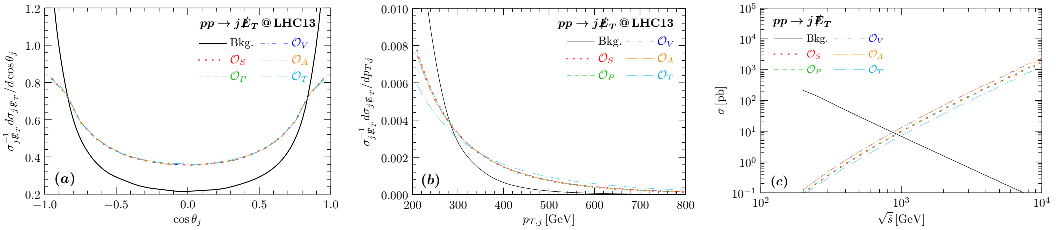

Mono-jet @Collider Search

Left panel: Validation of our simulation for the p_T^{recoil} distribution of the irreducible background channel $pp \to jZ(\nu\bar{\nu})$ at the LHC with a total luminosity $\mathcal{L} = 139\ fb^{-1}$. The experimental data (black dots) are taken from the paper arXiv:2102.10874 [hep-ex], and our results (red rectangles) have been renormalized by multiplying an overall constant.
Right panel: Expected exclusion limits at 95% C.L. at the LHC with $\sqrt{s} = 13 TeV$ and a total luminosity $\mathcal{L} = 139\ fb^{-1}$.

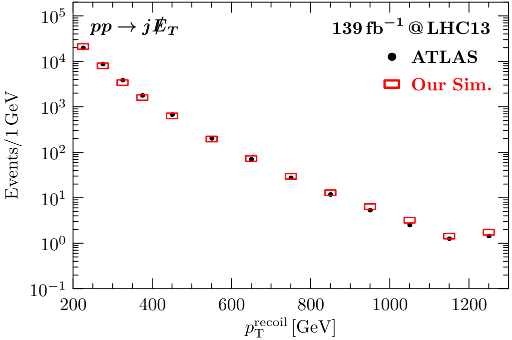

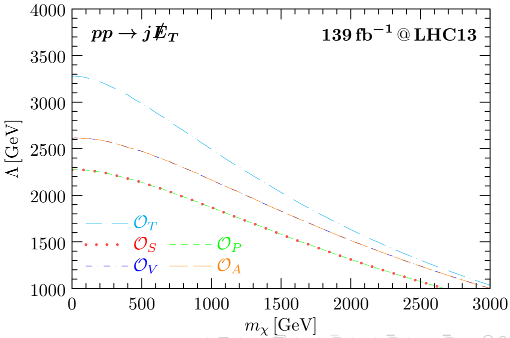

Mono-Z @Collider Search

Feynman diagrams contribute to the mono-Z events. **(a)** and **(b)** for the signal operators, **(c)** and **(d)** for the irreducible background.

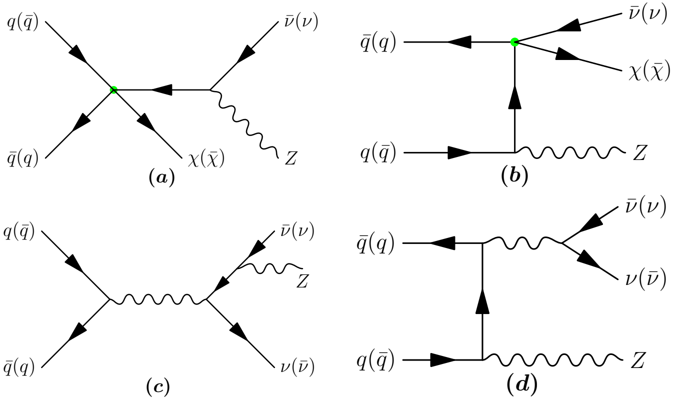

Reconstruction of the Z boson is needed in practice.

Leptonic Decay Modes @Mono-Z

Normalized distributions of the polar angle (θ_{Z_ℓ}, **left panel**) and the transverse momentum ($p_{T,Z}$, **right panel**) of the reconstructed Z boson from its leptonic decay modes. In both panels, the observables are calculated in the lab frame with center of mass energy $\sqrt{s} = 13TeV$, and the signal (colorful non-solid curves) are shown for parameters $m_\chi = 0GeV$ and $\Lambda_i = 1TeV$, the background (black-solid curve) stands for the irreducible contribution from the channel $q\bar{q} \to Z\nu\nu$.

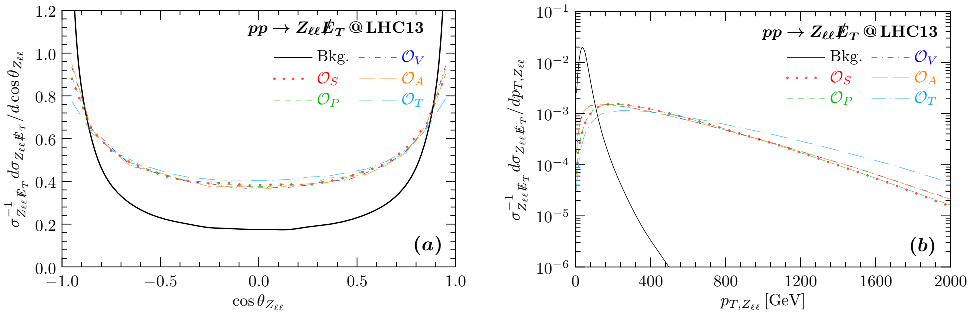

Leptonic Decay Modes @Mono-Z

Left panel: Normalized distribution of the transverse mass m_T . The distributions of the signals (colorful non-solid curves) are illustrated for parameters $m_\chi = 0\,GeV$ and $\Lambda_i = 1 TeV$. The background (black-solid curve) stands for the irreducible contribution from the channel $pp \to Z(\ell\ell)\nu\bar{\nu}$. **Right panel:** Validation of our simulation for the m_T distribution of the irreducible background at the LHC with center of mass energy $\sqrt{s} = 13 TeV$ and a total luminosity $\mathcal{L} = 139\ fb^{-1}$. The experimental data are (black dot) taken from arXiv:2111.08372 [hep-ex], and our results (red trangle) have been renormalized by multiplying an overall constant.

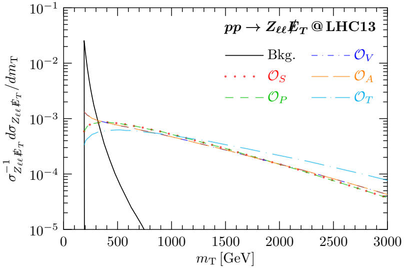

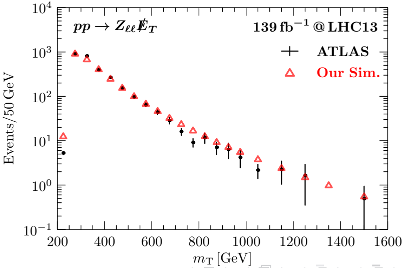

Leptonic Decay Modes @Mono-Z

Left panel: Validation of our simulation for the m_T distribution of the irreducible background. The experimental data are (black dot) taken from arXiv:2111.08372 [hep-ex]. **Right panel**: Expected exclusion limits at 95% C.L. using the mono-Z events at the LHC with center of mass energy $\sqrt{s} = 13\,TeV$ and a total luminosity $\mathcal{L} = 139\,fb^{-1}$. The Z-boson is reconstructed by its leptonic decay modes $Z \to \ell\ell$ with $\ell = e, \mu$.

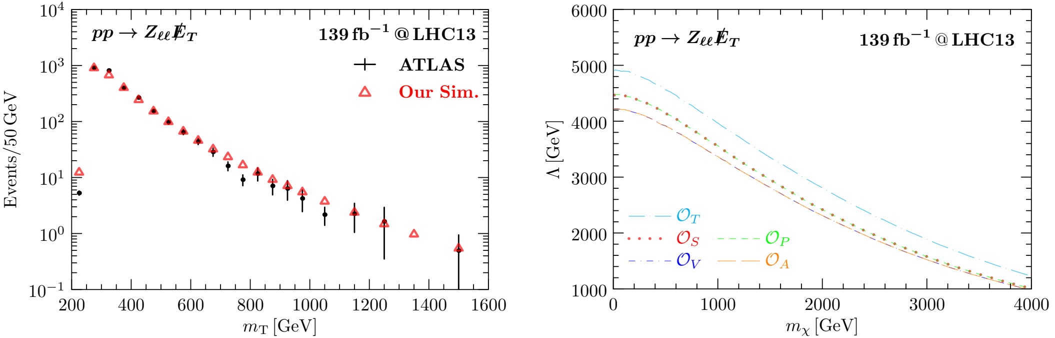

Hadronic Decay Modes @Mono-Z

Normalized polar angle (**left panel**) and transverse momentum (**right panel**) distributions of the reconstructed vector boson with invariant mass in the window $m_{jj} \in [65,\ 105]\,GeV$ for the sum of channels $pp \to V(jj) + \not{p}_T$ ($V = Z$ and W) at center-of-mass energy $\sqrt{s} = 13TeV$, respectively. For both panels, the signal events with parameters $m_\chi = 0\,GeV$ and $\Lambda_i = 1TeV$ are illustrated by colorful non-solid curves, and the background is shown by black-solid curve.

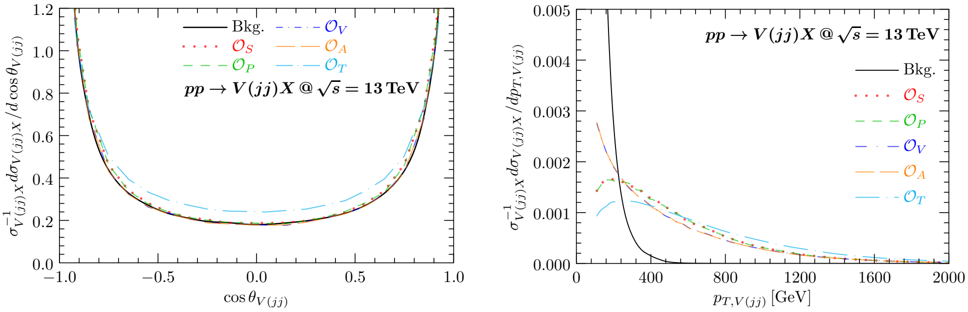

Hadronic Decay Modes @Mono-Z

Normalized polar angle **(a)** and the transverse momentum **(b)** distributions in the invariant mass window $m_{jets} \in [65,\ 105]\,GeV$ for the channels $pp \to \not{p}_T + jets$, respectively. For all the panels, the signal events (colorful non-solid curves) are illustrated with parameters $m_\chi = 0\,GeV$ and $\Lambda_i = 1\,TeV$.

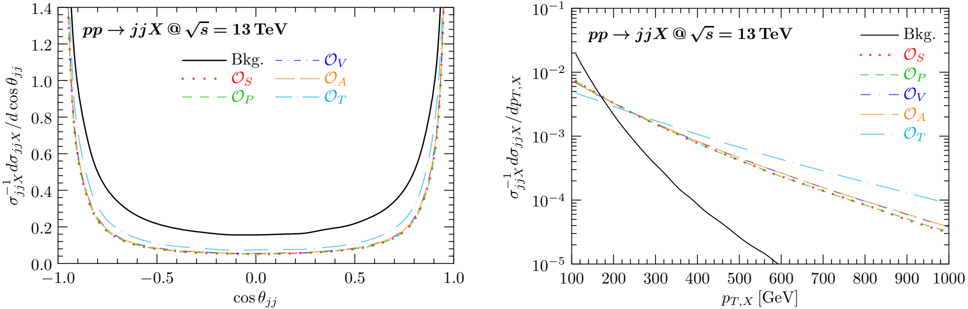

Hadronic Decay Modes @Mono-Z

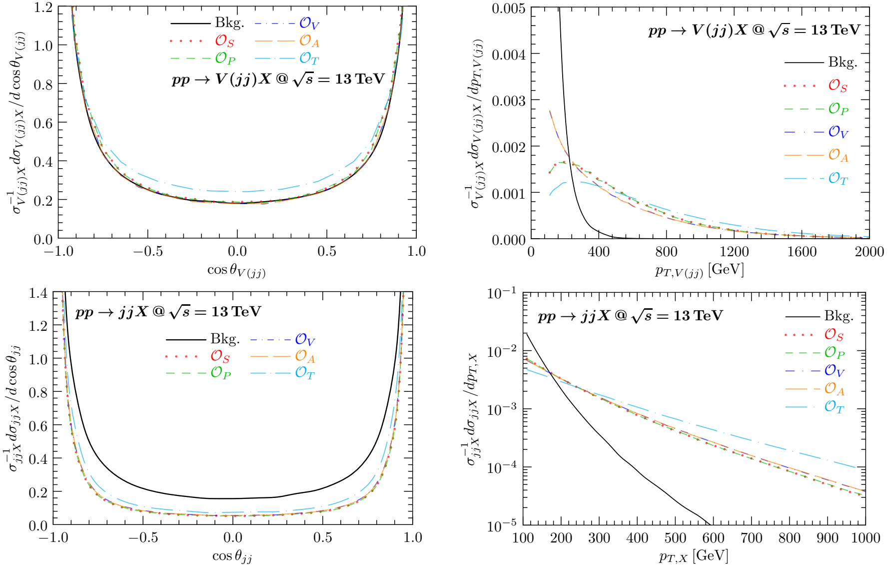

Hadronic Decay Modes @Mono-Z

Validation of our simulation for the missing transverse energy distribution of the pure QCD di-jet production channel $pp \to Z(\nu\nu) + jj$ at the LHC13 with a total luminosity $\mathcal{L} = 36.1\,fb^{-1}$. The **left** and **right panels** are for the HP and LP regions, respectively. The experimental data (black-solid line) are taken from arXiv:1807.11471 [hep-ex], and our results (red triangle) have been renormalized by multiplying an overall constant.

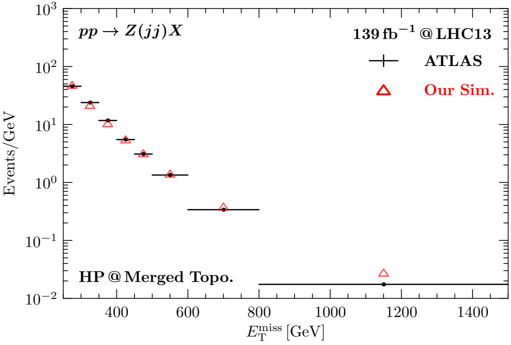

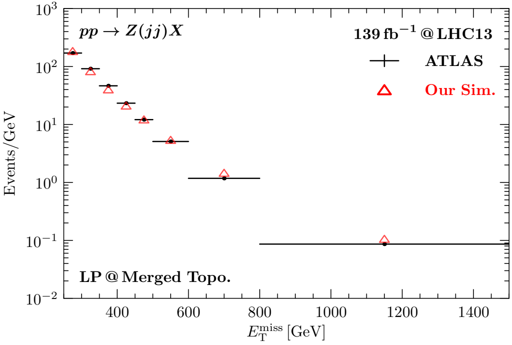

Hadronic Decay Modes @Mono-Z

Expected exclusion limits at 95% C.L. using the mono-$\mathcal{Z}/\mathcal{W}$ events with hadronically decaying $\mathcal{Z}/\mathcal{W}$ boson at the LHC with center of mass energy $\sqrt{s} = 13\mathcal{TeV}$ and a total luminosity $\mathcal{L} = 36.1\,fb^{-1}$. The **left** and **right panels** are for the HP and LP regions, respectively.

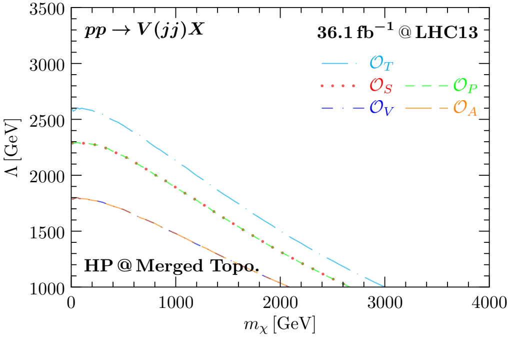

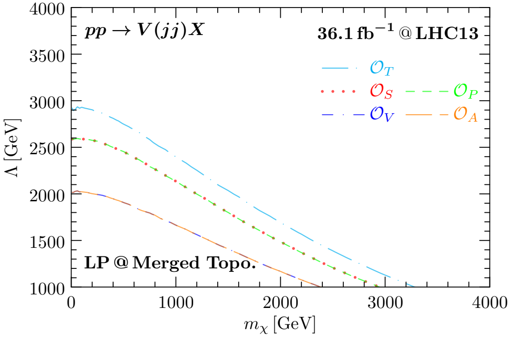

Nucleon Matrix Elements @Absorption

The parton-level operators induce nucleon-level interactions,

$$\langle \mathcal{N} | m_q \bar{q} q | \mathcal{N} \rangle = \mathcal{F}_S^{q/\mathcal{N}}(q^2) \bar{u}_\mathcal{N} u_\mathcal{N} , \tag{2}$$

$$\langle \mathcal{N} | m_q \bar{q} i\gamma_5 q | \mathcal{N} \rangle = \mathcal{F}_P^{q/\mathcal{N}}(q^2) \bar{u}_\mathcal{N} i\gamma_5 u_\mathcal{N} , \tag{3}$$

$$\langle \mathcal{N} | \bar{q} \gamma^\mu q | \mathcal{N} \rangle = \bar{u}_\mathcal{N} \left[\mathcal{F}_1^{q/\mathcal{N}}(q^2) \gamma^\mu + \frac{i\sigma^{\mu\nu} q_\nu}{2m_\mathcal{N}} \mathcal{F}_2^{q/\mathcal{N}}(q^2) \right] u_\mathcal{N} , \tag{4}$$

$$\langle \mathcal{N} | \bar{q} \gamma^\mu \gamma_5 q | \mathcal{N} \rangle = \bar{u}_\mathcal{N} \left[\mathcal{F}_A^{q/\mathcal{N}}(q^2) \gamma^\mu \gamma_5 + \frac{\gamma_5 q^\mu}{2m_\mathcal{N}} \mathcal{F}_{P'}^{q/\mathcal{N}}(q^2) \right] u_\mathcal{N} , \tag{5}$$

$$\langle \mathcal{N} | m_q \bar{q} \sigma^{\mu\nu} q | \mathcal{N} \rangle = \bar{u}_\mathcal{N} \left[\mathcal{F}_{T,0}^{q/\mathcal{N}}(q^2) \sigma^{\mu\nu} + \frac{i\gamma^{[\mu} q^{\nu]}}{2m_\mathcal{N}} \mathcal{F}_{T,1}^{q/\mathcal{N}}(q^2) + \frac{iq^{[\mu} p^{\nu]}}{m_\mathcal{N}^2} \mathcal{F}_{T,2}^{q/\mathcal{N}}(q^2) \right] u_\mathcal{N} , \tag{6}$$

where $p = p_f + p_i$ is sum of the nucleus momentum, and $q = p_f - p_i$ is the momentum transfer. For absorption process, $q^2 \approx m_\chi^2$

Spin-Independent @Absorption

The **scalar** and **vector** operators can induce spin-independent absorption. Excluded regions in the $m_\chi^2/4\pi\Lambda^4$-m_χ plan for the scalar operator (**left-panel**) and the vector operator (**right-panel**).

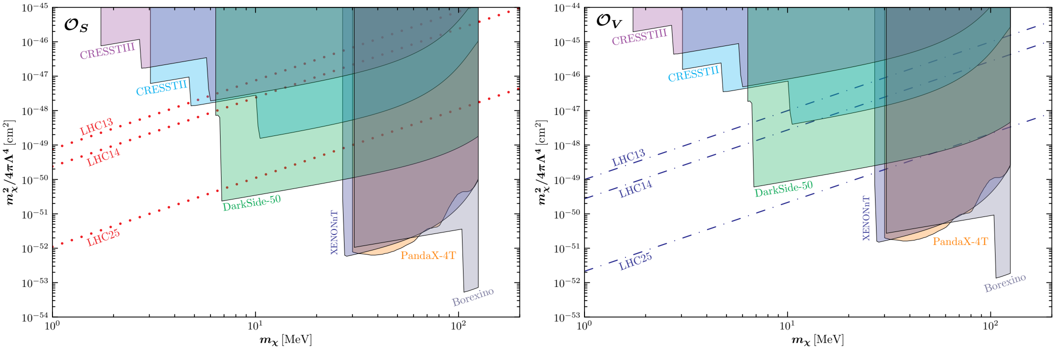

Experiment having lighter nucleus (Borexino, $C_6H_3(CH_3)_3$) is more sensitive

Spin-Dependent @Absorption

The **pseudo-scalar** and **axial-vector** operators can induce spin-dependent absorption. Excluded regions in the $m_\chi^2/4\pi\Lambda^4$-m_χ plan by the SD scatterings for the pseudo-scalar operator (**left-panel**) and the axial-vector operator (**right-panel**).

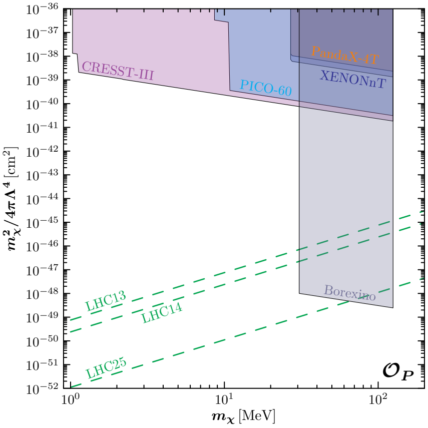

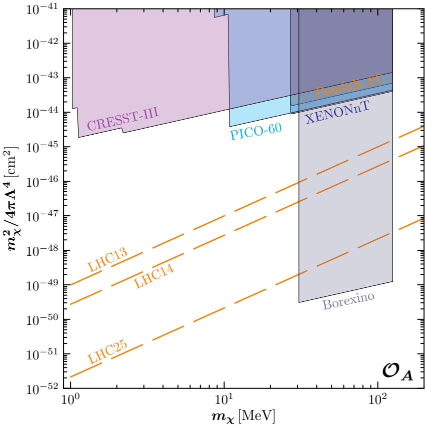

Tensor Operator @Absorption

The matrix elements include both SI and SD interactions,

$$\langle \mathcal{N} | m_q \bar{q} \sigma^{\mu\nu} q | \mathcal{N} \rangle = \bar{u}_{\mathcal{N}} \left[\mathcal{F}^{q/\mathcal{N}}_{\mathcal{T},0}(q^2) \sigma^{\mu\nu} + \frac{i\gamma^{[\mu} q^{\nu]}}{2m_{\mathcal{N}}} \mathcal{F}^{q/\mathcal{N}}_{\mathcal{T},1}(q^2) + \frac{iq^{[\mu} p^{\nu]}}{m^2_{\mathcal{N}}} \mathcal{F}^{q/\mathcal{N}}_{\mathcal{T},2}(q^2) \right] u_{\mathcal{N}} \,, \quad (7)$$

The total amplitude is the sum of these two kinds of contributions,

$$\mathcal{M}_{\mathcal{A},\mathcal{T}} = \mathcal{M}^{\mathcal{SD}}_{\mathcal{A},\mathcal{T}} + \mathcal{M}^{\mathcal{SI}}_{\mathcal{A},\mathcal{T}} \,. \quad (8)$$

In our case, the interference contribution is given as,

$$\overline{\Re\{\mathcal{M}^{\dagger}_{\mathcal{T},\mathcal{SD}} \mathcal{M}_{\mathcal{T},\mathcal{SI}}\}} \propto \sum_{\mathcal{M}} \left\langle \mathcal{J}, \mathcal{M} \left| \boldsymbol{q} \cdot \mathcal{S}_{\mathcal{N}} \right| \mathcal{J}, \mathcal{M} \right\rangle \,. \quad (9)$$

Since the nuclear target is unpolarized and orientation of the momentum transfer (or equivalently the DM velocity) is universal in all directions, the total contribution of the interference term is zero in average.

Tensor Operator @Absorption

Excluded regions in the $m_\chi^2/4\pi\Lambda^4$-m_χ plan by the SD scatterings for the tensor operator.

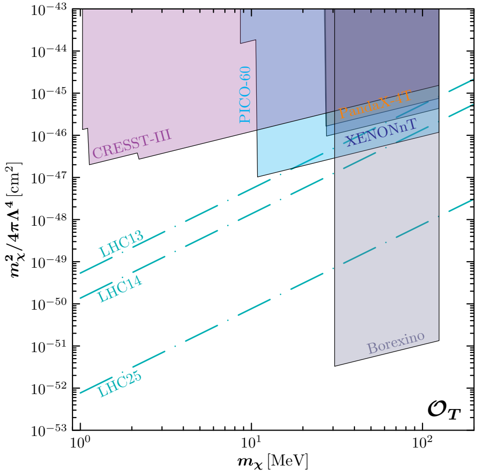

The SI contribution is suppressed by a factor of $m_\chi^2/m_{\mathcal{A}}^2$, but receives an enhancement factor $\mathcal{A}^2$ which can be large for heavier nuclear target. The total scale factor is hence,

$$\frac{m_\chi^2}{m_{\mathcal{A}}^2}\mathcal{A}^2 \approx \frac{m_\chi^2}{\mathcal{A}^2 m_{\mathcal{N}}^2}\mathcal{A}^2 = \frac{m_\chi^2}{m_{\mathcal{N}}^2} \tag{7}$$

This factor can be sizable for light nuclear target and a relatively heavier DM.

However, since we are interested in the DM with $m_\chi \lesssim 100\,\mathcal{MeV}$, the net enhancement is negligible in our case.

Summary

- We studied mono-X signatures of the four-fermion contact interactions at hadron colliders.
- The mono-Z production with a leptonic decay Z boson provides the strongest bound.
- For scalar and vector operators, the SI absorption can give stronger constraints for $m_\chi \in [10,\ 100]\,\mathcal{M}eV$ (**lighter nucleus can give better**).
- For pseudo-scalar, axial-vector and tensor operators, the SD absorption at **lighter nucleus** can give stronger constraints for $m_\chi \in [10,\ 100]\,\mathcal{M}eV$.

Thank you very much for your attention!